A robust power spectrum split cancellation-based spectrum sensing method for cognitive radio systems*

Qi Pei-Han(齐佩汉)†, Li Zan(李 赞), Si Jiang-Bo(司江勃), and Gao Rui(高 锐)

State Key Laboratory of Integrated Service Networks, Xidian University, Xi'an 710071, *China*

(Received 17 April 2014; revised manuscript received 26 June 2014; published online 10 October 2014)

Spectrum sensing is an essential component to realize the cognitive radio, and the requirement for real-time spectrum sensing in the case of lacking prior information, fading channel, and noise uncertainty, indeed poses a major challenge to the classical spectrum sensing algorithms. Based on the stochastic properties of scalar transformation of power spectral density (PSD), a novel spectrum sensing algorithm, referred to as the power spectral density split cancellation method (PSC), is proposed in this paper. The PSC makes use of a scalar value as a test statistic, which is the ratio of each subband power to the full band power. Besides, by exploiting the asymptotic normality and independence of Fourier transform, the distribution of the ratio and the mathematical expressions for the probabilities of false alarm and detection in different channel models are derived. Further, the exact closed-form expression of decision threshold is calculated in accordance with Neyman–Pearson criterion. Analytical and simulation results show that the PSC is invulnerable to noise uncertainty, and can achive excellent detection performance without prior knowledge in additive white Gaussian noise and flat slow fading channels. In addition, the PSC benefits from a low computational cost, which can be completed in microseconds.

Keywords: spectrum sensing, power spectral density, noise uncertainty, real time

PACS: 84.40.Ua **DOI:** 10.1088/1674-1056/23/12/128401

1. Introduction

The rapid growth in wireless communications has brought about conflicts between a huge demand on the deployment of new wireless services and increasingly scarce spectrum resources. However, various researches of spectrum utilization have shown that substantial resources in frequency, time, and space are inefficiently exploited, even unused.[1,2] To address this problem, cognitive radio (CR)[3–5] has emerged as a promising technology to enable the access of the intermittent periods of unoccupied frequency bands, and thereby increases the spectral efficiency. In the most primitive sense, the fundamental task of secondary users (SUs) in CR networks is to detect the primary users (PUs). This is usually achieved by sensing the ambient radio frequency environments of SUs, a process called spectrum sensing.[6–9] In practical CR networks applications, spectrum sensing usually has to suffer the following afflictions.

(i) Spectrum sensing needs to be able to detect PUs at a fairly low detection signal-to-noise ratio (SNR) level with low detection error probabilities.[10]

(ii) Given the protection for PUs and the inaccurateness of estimating parameters in the low SNR regime, spectrum sensing should work well without any cofactor.[11]

(iii) Complex electromagnetic environments such as multipath fading, shadowing, and the noise uncertainty may seriously compromise the performance of spectrum sensing.

(iv) The spectrum sensing time interval must be limited at an acceptable level, or it will lead to low spectrum utilization. More importantly, SUs will bring harmful interference to reappeared PUs.

To cope with the challenges mentioned above, several spectrum sensing schemes have been proposed in the literature. When SUs have perfect knowledge of the signal waveform of PUs, the optimal spectrum sensing method is coherent detection,[12] as it maximizes the signal-to-noise ratio (SNR) at the detector's output. However, coherent detection is almost ineffective in blind spectrum sensing. By exploiting the cyclostationary feature from modulation type, carrier frequency, symbol rate, and sampling rate of the PU signal, cyclostationary-based spectrum sensing[13] achieves reliable performance, even in the very low SNR regime. As a drawback, it often requires a prior knowledge of the signal characteristics to reduce the computational complexity. Given that the statistical covariance matrices or autocorrelations of the signal and noise are generally different, eigenvalue-based spectrum sensing methods are proposed in Refs. [14]–[18]. These methods have wide applications in signal detection without requiring knowledge of the signal, channel, and noise power. Nevertheless, it is very difficult (mathematically intractable) to obtain a precisely closed-form formula for the threshold. Although some improvements have been made for this issue in Refs. [17] and [18], it is still not easy to apply to practical scenarios, since optimal thresholds depend on empirical values. Due to its advantages of easy implementation, real

*Project supported by the National Natural Science Foundation of China (Grant No. 61301179), the Doctorial Program Foundation of the Ministry of Education, China (Grant No. 20110203110011), and the 111 Project, China (Grant No. B08038).

†Corresponding author. E-mail: qipeihan@126.com

© 2014 Chinese Physical Society and IOP Publishing Ltd

time, and blind spectrum sensing supported, energy detection (ED)[19–25] has been widely regarded as the most popular spectrum sensing technique in both study and application. ED can be performed in the time or frequency domain. Time-domain energy detection (TDED)[19,20] adds up the square modulus of the signal amplitude in the sensing period as the test statistic, while frequency-domain energy detection (FDED)[21–24] accumulates a power spectrum in the sensing bandwidth as the test statistic. Regardless of TDED or FDED, they have their own inherent limitation: noise uncertainty. Since the ED threshold depends on the noise variance, even a little noise uncertainty may affect ED performance seriously.[25]

Inspired by some FDED methods,[21–24] a power spectral density split cancellation (PSC) method is proposed in this paper. In contrast to FDED, the PSC uses the ratio of each subband power to the full band power as a test statistic. Benefitting from this scalar transformation, the PSC not only inherits the advantages of FDED, but also overcomes the impact of noise uncertainty. The novel contribution of this paper is as follows.

i) Based on the asymptotic normality and independence of Fourier transform, we first get the stochastic properties of the power spectral density, and then we calculate the cumulative distribution function of the ratio of each subband power to the full band power. In addition, the exact closed-form expressions of the probability of a false alarm and the decision threshold are obtained. Most importantly, it is shown that the decision threshold is just decided by the configuration parameters of the PSC, and theoretically, we prove that the PSC is inherently capable of suppressing the noise uncertainty.

ii) Considering the correlation of oversampling samples, a more accurate mathematical formula for the probability of detection under additive white Gaussian noise (AWGN) channel and flat slow fading channels are derived. Both analytical and simulation results show that the PSC could offer a high probability of detection at a low probability of a false alarm for a wide range of SNR without prior knowledge in different channels. These conclusions can give important insight into the performance of this algorithm under various channel models and operational scenarios.

iii) Algorithm complexity is analyzed according to the PSC procedure, and we verify that the Fourier transform dominates the computation overhead of the PSC. When implemented on a Field-Programmable Gate Array (FPGA), the PSC will be accomplished in microseconds by means of mature module of fast Fourier transform techniques.

The rest of this paper is organized as follows. Section 2 presents the employed system model. In Section 3, the steps of the PSC are summarized and the expressions for the probability of detection and a false alarm are derived. Section 4 provides atheoretical performance analysis in four aspects. In Section 5, we illustrate the performance of the proposed method via some simulations. Finally, we conclude our paper in Section 6.

2. System model and basic assumptions

In this section, a reasonable system model considering signal oversampling is presented, which serves as an analysis basis to study blind spectrum sensing. The single-user spectrum sensing is formulated as a binary hypothesis problem as follows:

$$x(t)=\begin{cases} w(t), & \mathscr{H}_0, \\ h(t)s(t)+w(t), & \mathscr{H}_1. \end{cases} \tag{1}$$

We make the following assumptions:

AS1 $x(t)$ denotes the received signal at the SU, $s(t)$ is a PU transmitted signal, which is unknown and real, $\omega(t)$ is band-limited white noise, $h(t)$ is the channel coefficient, which is independent of $\omega(t)$, $\mathscr{H}_0$ and $\mathscr{H}_1$ denote the hypothesis of the absence and the presence of the PU signal respectively;

AS2 $\omega(t)$ is the complex Gaussian, independently and identically distributed (i.i.d.) random process with mean zero and variance σ_ω^2, namely $\omega(t)\sim\mathscr{CN}(0,\sigma_\omega^2)$, and it can be denoted as $\omega(t)=\omega^{\mathrm{r}}(t)+\mathrm{j}\omega^{\mathrm{i}}(t)$, where $\omega^{\mathrm{r}}(t)$ and $\omega^{\mathrm{i}}(t)$ are the real part and imaginary part of $\omega(t)$, $\omega^{\mathrm{r}}(t)$, and $\omega^{\mathrm{i}}(t)$ is the independent Gaussian random process with mean zero and variance $\sigma_\omega^2/2$;

AS3 $h(t)$ could be either a constant or complex random process, with mean μ_h and variance σ_h^2. Without considerations of large scale fading and shadowing, we have $\mu_h^2+\sigma_h^2=1$. When the PU signal transmits in the AWGN channel, $h(t)$ is constant and $\mu_h=1$; when the PU signal transmits in the slow flat fading channel, $h(t)$ is a complex random process and it will remain unchanged for at least a symbol period. In this paper, we assume $h(t)$ stays unchanged in a symbol period, and we discuss two classic slow flat fading channels:

1) **Rayleigh channel**: $h(t)$ is complex Gaussian random process with $\mu_h=0$ and $\sigma_h^2=1$.

2) **Rician channel**: $h(t)$ is complex Gaussian random process with $K=\mu_h^2/\sigma_h^2$, and Rician factor K is the ratio between the power in the direct path and the power in the other scattered paths.

For the evaluation of the detection performance, the probabilities of detection P_{d} and false alarm P_{f} are defined as

$$P_{\mathrm{d}}=P\{\text{decision}=\mathscr{H}_1|\mathscr{H}_1\}, \tag{2}$$

$$P_{\mathrm{f}}=P\{\text{decision}=\mathscr{H}_1|\mathscr{H}_0\}. \tag{3}$$

Discrete observations $x(n), n=0,1,\ldots,N-1$ are sampled from received signal $x(t)$, with N denoting the total number of discrete samples. From the above assumptions, samples $x(n), n=0,1,\ldots,N-1$ will be equal to $\omega(n), n=0,1,\ldots,N-1$ when PU is absent, whereas they will be equal to $h(n)s(n)+$

$\omega(n), n = 0, 1, ..., N-1$. In addition, $x(n)$ is a random variable, which obeys a complex Gaussian distribution

$$x(n) \sim \begin{cases} \mathscr{CN}(0, \sigma_\omega^2), & \mathscr{H}_0, \\ \mathscr{CN}(\mu_h s(n), \sigma_h^2 s^2(n) + \sigma_\omega^2), & \mathscr{H}_1, \end{cases} \tag{4}$$

where $h(n)$, $s(n)$, and $\omega(n)$ are the discrete sample of $h(t)$, $s(t)$, and $\omega(t)$, respectively.

In realistic blind spectrum sensing scenarios, because of lacking prior information, the sampling rate has to be determined by the instantaneous monitoring bandwidth (IMBW) of the receiver rather than the bandwidth of the PU signal, and usually it is twice or multiple of the IMBW. We assume that the PU signal may appear in the IMBW, and the signal bandwidth is less than IMBW. Thus, oversampling towards the PU signal will take place inevitably. When analyzing the statistic characteristics of the PSC, we should consider the influence brought by oversampling.

3. Single-user PSC

In this section, firstly, the flow of the single-user PSC will be given, and the asymptotic normality and independence of Fourier transform are confirmed. Secondly, the stochastic properties of PSD are deduced. Finally, the mathematical expression for the probability of a false alarm is derived, and we infer an exact closed-form expression of the decision threshold of the PSC.

3.1. The PSC algorithm

The discrete samples $x(n)$, $n = 0, 1, ..., N-1$ will be divided into U segments with the same length M. The u-th segment is $x_u(n)$, $n = 0, 1, ..., M-1$, $u = 1, 2, ..., U$. Here the segment length M is chosen as even and $M = N/U$. Considering the difference of the stochastic properties of the power spectral density between $\mathscr{H}_1$ and $\mathscr{H}_0$, the test statistic of the PSC is designed in use of normalized PSD and the PSC can be summarized as five steps given below.

Step 1 Calculating the Fourier transform of $x_u(n)$

$$X_u(k) = \frac{1}{\sqrt{M}} \sum_{n=0}^{M-1} x_u(n)\, \mathrm{e}^{-2\pi \mathrm{j} kn/M}, \tag{5}$$

where $k = 0, 1, ..., M-1$ and $u = 1, 2, ..., U$.

Step 2 Getting the power spectrum $F_u(k)$ by the periodogram method

$$F_u(k) = |X_u(k)|^2, \tag{6}$$

so the average power spectrum of all the segments can be expressed as

$$F_{\text{avg}}(k) = \frac{1}{U} \sum_{u=1}^{U} F_u(k), \tag{7}$$

where $k = 0, 1, ..., M-1$ and $u = 1, 2, ..., U$. Given the transmitted signal is real, its power spectrum is symmetric. For convenience, we only use the power spectrum of positive frequency.

Step 3 Splitting the power spectrum into L subbands with $T/2$ frequency bins in each subband, where L is a positive integer. Then the power of full band and subband can be obtained from the following expression

$$F_{\text{full}} = \sum_{k=1}^{M/2} F_{\text{avg}}(k), \tag{8}$$

$$F_l = \sum_{k=1}^{T/2} F_{\text{avg}}((l-1)\frac{T}{2} + k), \tag{9}$$

where $l = 1, 2, ..., L$.

Step 4 Generating the test statistic $r(l)$ for each subband by introducing normalization to take scalar transformation

$$r(l) = \frac{F_l}{F_{\text{full}}}, \quad l = 1, 2, ..., L. \tag{10}$$

Step 5 Comparing $r(l)$ with the threshold γ, if $r(l) \geq \gamma$, we set decision array element $R(l)$ as 1, otherwise $R(l) = 0$. The final decision is made as follows:

$$\begin{cases} \sum_{l=1}^{L} R(l) = 0, & \text{decide } \mathscr{H}_0, \\ \sum_{l=1}^{L} R(l) \geq 1, & \text{decide } \mathscr{H}_1. \end{cases} \tag{11}$$

3.2. Stochastic properties of power spectral density

To get the distribution of the test statistic, we first derive the stochastic properties of PSD $F_u(k)$. To facilitate analysis, Fourier transform of $x_u(n)$ in Step 1 is decomposed into

$$X_u(k) = X_u^{\text{r}}(k) + \mathrm{j} X_u^{\text{i}}(k), \tag{12}$$

where $X_u^{\text{r}}(k)$ and $X_u^{\text{i}}(k)$ are the real part and imaginary part of $X_u(k)$. So, PSD estimation in Eq. (6) can be written as $F_u(k) = (X_u^{\text{r}}(k))^2 + (X_u^{\text{i}}(k))^2$. To analyze the stochastic properties of $F_u(k)$, we should derive the distributions and the covariance of $X_u^{\text{r}}(k)$ and $X_u^{\text{i}}(k)$ along with the covariance of $X_u(p)$ and $X_u(q)$, where $0 \leq p, q \leq M-1, p \neq q$.

Under $\mathscr{H}_0$, by substituting $x_u(n) = \omega_u^{\text{r}}(n) + \mathrm{j}\omega_u^{\text{i}}(n)$ into Eq. (5), the real part $X_u^{\text{r}}(k)$ can be expressed as

$$\begin{aligned} X_u^{\text{r}}(k) = & \frac{1}{\sqrt{M}} \sum_{n=0}^{M-1} \left[\cos\left(\frac{2\pi kn}{M}\right) \omega_u^{\text{r}}(n) \right] \\ & + \frac{1}{\sqrt{M}} \sum_{n=0}^{M-1} \left[\sin\left(\frac{2\pi kn}{M}\right) \omega_u^{\text{i}}(n) \right]. \end{aligned} \tag{13}$$

Similarly, the imaginary part $X_u^{\text{i}}(k)$ is

$$\begin{aligned} X_u^{\text{i}}(k) = & \frac{1}{\sqrt{M}} \sum_{n=0}^{M-1} \left[\cos\left(\frac{2\pi kn}{M}\right) \omega_u^{\text{i}}(n) \right] \\ & - \frac{1}{\sqrt{M}} \sum_{n=0}^{M-1} \left[\sin\left(\frac{2\pi kn}{M}\right) \omega_u^{\text{r}}(n) \right]. \end{aligned} \tag{14}$$

When the sample rate is multiple times of IMBW, which is the practical noise bandwidth, $\omega(n), n = 0,1,...,N-1$ are independent of each other. Along with the independence between $\omega_u^{\mathrm{r}}(n)$ and $\omega_u^{\mathrm{i}}(n)$, the mean and variance of $X_u^{\mathrm{r}}(k)$ and $X_u^{\mathrm{i}}(k)$ can be directly achieved as

$$E\left[X_u^{\mathrm{r}}(k)\right] = E\left[X_u^{\mathrm{i}}(k)\right] = 0, \tag{15}$$

$$D\left[X_u^{\mathrm{r}}(k)\right] = D\left[X_u^{\mathrm{i}}(k)\right] = \frac{\sigma_\omega^2}{2}, \tag{16}$$

where $E[\cdot]$ and $D[\cdot]$ stand for mean and variance operators. By the following lemma, we can know the covariance of $X_u^{\mathrm{r}}(k)$ and $X_u^{\mathrm{i}}(k)$.

Lemma 1 Under $\mathscr{H}_0$, the covariance of $X_u^{\mathrm{r}}(k)$ and $X_u^{\mathrm{i}}(k)$ is zero

$$\mathrm{Cov}\left[X_u^{\mathrm{r}}(k), X_u^{\mathrm{i}}(k)\right] = 0. \tag{17}$$

Proof According to Eq. (15), the covariance between $X_u^{\mathrm{r}}(k)$ and $X_u^{\mathrm{i}}(k)$ under $\mathscr{H}_0$ can be simplified as

$$\begin{aligned}
&\mathrm{Cov}\left[X_u^{\mathrm{r}}(k), X_u^{\mathrm{i}}(k)\right] \\
&= E\left[\left(X_u^{\mathrm{r}}(k) - E\left(X_u^{\mathrm{r}}(k)\right)\right)\left(X_u^{\mathrm{i}}(k) - E\left(X_u^{\mathrm{i}}(k)\right)\right)\right] \\
&= E\left[X_u^{\mathrm{r}}(k) X_u^{\mathrm{i}}(k)\right].
\end{aligned} \tag{18}$$

Substituting Eqs. (13) and (14) into Eq. (18), we have

$$\begin{aligned}
&\mathrm{Cov}\left[X_u^{\mathrm{r}}(k), X_u^{\mathrm{i}}(k)\right] \\
&= \frac{1}{M}\sum_{n=0}^{M-1} \cos\left(\frac{2\pi kn}{M}\right)\sin\left(\frac{2\pi kn}{M}\right) E\left[\omega_u^{\mathrm{i}}(n)^2\right] \\
&\quad - \frac{1}{M}\sum_{n=0}^{M-1} \cos\left(\frac{2\pi kn}{M}\right)\sin\left(\frac{2\pi kn}{M}\right) E\left[\omega_u^{\mathrm{r}}(n)^2\right] \\
&= 0.
\end{aligned} \tag{19}$$

As shown in the following lemma, we derive the correlation of the power spectrum of different frequency bins from the same segment under $\mathscr{H}_0$.

Lemma 2 Under $\mathscr{H}_0$, the power spectrums of different bins from the same segment are uncorrelated, that is

$$\mathrm{Cov}\left[X_u(p), X_u(q)\right] = 0, \quad (p \neq q, 0 \leq p, q \leq M-1). \tag{20}$$

Proof From Eq. (15), it is obviously to get

$$E\left[X_u(p)\right] = E\left[X_u(q)\right] = 0. \tag{21}$$

Then the covariance between $X_u(p)$ and $X_u(q)$ can be expressed as

$$\begin{aligned}
&\mathrm{Cov}[X_u(p), X_u(q)] \\
&= E\left[\overline{\langle X_u(p) - E\left(X_u(p)\right)\rangle}\,\langle X_u(q) - E\left(X_u(q)\right)\rangle\right] \\
&= E\left[\left(\overline{\frac{1}{\sqrt{M}}\sum_{n=0}^{M-1}\exp\left(-\frac{2\pi \mathrm{j} pn}{M}\right)\omega_u(n)}\right)\right. \\
&\quad \left.\times\left(\frac{1}{\sqrt{M}}\sum_{n'=0}^{M-1}\exp\left(-\frac{2\pi \mathrm{j} qn'}{M}\right)\omega_u(n')\right)\right] \\
&= \frac{1}{M}\sum_{n=0}^{M-1}\exp\left(\frac{2\pi \mathrm{j}(p-q)n}{M}\right) E\left[\omega_u^2(n)\right].
\end{aligned} \tag{22}$$

From the formula for the sum of a geometric series, we obtain

$$\begin{aligned}
&\mathrm{Cov}\left[X_u(p), X_u(q)\right] \\
&= \sum_{n=0}^{M-1}\exp\left[\mathrm{j}\frac{2\pi}{M}(p-q)n\right] E\left[\omega_u^2(n)\right] \\
&= 0, \quad p \neq q, 0 \leq p, q \leq M-1.
\end{aligned} \tag{23}$$

Thus, different power spectrum bins of the same segment are uncorrelated.

With the help of Lemma 1 and Lemma 2, the following theorem can be given.

Theorem 1 Under $\mathscr{H}_0$, the power spectrums $F_u(k), 0 \leq k \leq M-1$ are independent, which obey a central Chi-square distribution with two degrees of freedom. The mean and variance of $F_u(k)$ are

$$E\left[F_u(k)|\mathscr{H}_0\right] = \sigma_\omega^2, \tag{24}$$

$$D\left[F_u(k)|\mathscr{H}_0\right] = \sigma_\omega^4. \tag{25}$$

Proof As is known to all, the Fourier transform is a linear transformation, so the Fourier transform of $\omega_u(n)$ is also a Gaussian distribution. In addition, the real part $X_u^{\mathrm{r}}(k)$ and imaginary part $X_u^{\mathrm{i}}(k)$ of $X_u(k)$ also obey a Gaussian distribution. Using Lemma 1, we will know that $X_u^{\mathrm{r}}(k)$ and $X_u^{\mathrm{i}}(k)$ are independent. So, under $\mathscr{H}_0$, $F_u(k)$ obeys a central Chi-square distribution with two degrees of freedom. The mean and variance of $F_u(k)$ can be achieved as

$$E\left[F_u(k)|\mathscr{H}_0\right] = 2\left(\sqrt{\frac{\sigma_\omega^2}{2}}\right)^2 = \sigma_\omega^2, \tag{26}$$

$$D\left[F_u(k)|\mathscr{H}_0\right] = 4\left(\sqrt{\frac{\sigma_\omega^2}{2}}\right)^4 = \sigma_\omega^4. \tag{27}$$

From Lemma 2, we can get that $X_u(p)$ and $X_u(q)$ are independent of each other. Since the continuous function of two independent variables is also independent, we could conclude that power spectrums $F_u(k) = |X_u(k)|^2$ are independent of different k.

When analyzing the stochastic properties of PSD under $\mathscr{H}_1$, the influence on the independence of $h(n)$, which is caused by oversampling, has been taken into consideration. In a slow flat fading channel, channel coefficient $h(n)$ from a certain change period is supposed to be one and the same random variable, and channel coefficients from different symbol periods are independent random variables. Oversampling factor R is defined as the ratio of sample rate to symbol rate, which is a positive integer $R \ll M$.

Under $\mathscr{H}_1$, by replacing $x_u(n)$ with $[h_u^{\mathrm{r}}(n)s_u(n)+\omega_u^{\mathrm{r}}(n)]+\mathrm{j}[h_u^{\mathrm{i}}(n)s_u(n)+\omega_u^{\mathrm{i}}(n)]$ in Eq. (5), the real part $X_u^{\mathrm{r}}(k)$ can be written as

$$X_u^{\mathrm{r}}(k) = \frac{1}{\sqrt{M}}\sum_{n=0}^{M-1}\left[\cos\left(\frac{2\pi kn}{M}\right)\left(h_u^{\mathrm{r}}(n)s_u(n)+\omega_u^{\mathrm{r}}(n)\right)\right] + \frac{1}{\sqrt{M}}\sum_{n=0}^{M-1}\left[\sin\left(\frac{2\pi kn}{M}\right)\left(h_u^{\mathrm{i}}(n)s_u(n)+\omega_u^{\mathrm{i}}(n)\right)\right], \tag{28}$$

and the imaginary part $X_u^{\mathrm{i}}(k)$ is

$$X_u^{\mathrm{i}}(k) = \frac{1}{\sqrt{M}}\sum_{n=0}^{M-1}\left[\cos\left(\frac{2\pi kn}{M}\right)\left(h_u^{\mathrm{i}}(n)s_u(n)+\omega_u^{\mathrm{i}}(n)\right)\right] - \frac{1}{\sqrt{M}}\sum_{n=0}^{M-1}\left[\sin\left(\frac{2\pi kn}{M}\right)\left(h_u^{\mathrm{r}}(n)s_u(n)+\omega_u^{\mathrm{r}}(n)\right)\right], \tag{29}$$

where $h_u^{\mathrm{r}}(n)$ and $h_u^{\mathrm{i}}(n)$ denote the real part and imaginary parts of $h_u(n)$, repectively.

In analogy to the analysis process mentioned above, we get the following lemmas about the distributions and correlation of $X_u^{\mathrm{r}}(k)$ and $X_i^{\mathrm{r}}(k)$ under $\mathscr{H}_1$.

Lemma 3 Under $\mathscr{H}_1$, the mean and variance of $X_u^{\mathrm{r}}(k)$ and $X_i^{\mathrm{r}}(k)$ are

$$E\left[X_u^{\mathrm{r}}(k)\right] = \frac{1}{\sqrt{M}}\mu_h^{\mathrm{r}}S_u^{\mathrm{r}}(k)+\frac{1}{\sqrt{M}}\mu_h^{\mathrm{i}}S_u^{\mathrm{i}}(k), \tag{30}$$

$$E\left[X_u^{\mathrm{i}}(k)\right] = \frac{1}{\sqrt{M}}\mu_h^{\mathrm{i}}S_u^{\mathrm{r}}(k)-\frac{1}{\sqrt{M}}\mu_h^{\mathrm{r}}S_u^{\mathrm{i}}(k), \tag{31}$$

$$D\left[X_u^{\mathrm{r}}(k)\right] = D\left[X_u^{\mathrm{i}}(k)\right] = \frac{\sigma_\omega^2}{2}+\frac{\sigma_h^2 G(k)}{2M}, \tag{32}$$

where $S_u(k)=\sum_{n=0}^{M-1}s_u(n)\,\mathrm{e}^{-\mathrm{j}2\pi kn/M}$, $S_u^{\mathrm{r}}(k)$ and $S_u^{\mathrm{i}}(k)$ are the real part and imaginary part of $S_u(k)$, and

$$G(k)=\sum_{n'=0}^{M/R-1}\left|\sum_{n=0}^{R-1}s_u(Rn'+n)\exp\left(-\frac{2\pi\mathrm{j}kn}{M}\right)\right|^2. \tag{33}$$

Proof See Appendix A.

Although the formulas in Lemma 3 are deduced in a slow flat fading channel, they are also suitable for an AWGN channel when σ_h^2 is replaced by value 0. In the following lemma, the correlation analysis of $X_u^{\mathrm{r}}(k)$ and $X_u^{\mathrm{i}}(k)$ under $\mathscr{H}_1$ is given.

Lemma 4 Under $\mathscr{H}_1$, the covariance of $X_u^{\mathrm{r}}(k)$ and $X_u^{\mathrm{i}}(k)$ are zero

$$\mathrm{Cov}\left[X_u^{\mathrm{r}}(k),X_u^{\mathrm{i}}(k)\right]=0. \tag{34}$$

Proof See Appendix B.

The following lemma discusses the correlation of different power spectrum bins under $\mathscr{H}_1$.

Lemma 5 Under $\mathscr{H}_1$, the power spectrum bins of the same segment are asymptotically uncorrelated, and the correlation coefficient of different spectrum bins meets

$$0\le|\rho|\le\frac{\sigma_h^2}{\sigma_h^2+1/\mathrm{SNR}}. \tag{35}$$

Proof See Appendix C. Obviously, the correlation coefficient of different spectrum bins in the AWGN channel is zero, as σ_h^2 equals zero in this channel model. In the slow flat fading channels, although σ_h^2 is not zero, we can also deduce that the correlation coefficient ρ tends to zero asymptotically when taking a low SNR regime of cognitive radio into account. So, different power spectrum bins of the same segment are asymptotically uncorrelated under $\mathscr{H}_1$.

Theorem 2 Under $\mathscr{H}_1$, the power spectrums $F_u(k), 0\le k\le M-1$ are asymptotically independent, which obey a noncentral Chi-square distribution with two degrees of freedom. The mean and variance of $F_u(k)$ are

$$E\left[F_u(k)|\mathscr{H}_1\right] = \frac{\mu_h^2|S_u(k)|^2+G(k)\sigma_h^2}{M}+\sigma_\omega^2, \tag{36}$$

$$D\left[F_u(k)|\mathscr{H}_1\right] = \frac{\left(G(k)\sigma_h^2+M\sigma_\omega^2\right)^2}{M^2} + \frac{2\mu_h^2|S_u(k)|^2\left(G(k)\sigma_h^2+M\sigma_\omega^2\right)}{M^2}. \tag{37}$$

Proof In the same way, from Eq. (4), we can conclude the Fourier transform $X_u(k)$, the real part $X_u^{\mathrm{r}}(k)$ and imaginary part $X_u^{\mathrm{i}}(k)$ all obey a Gaussian distribution. With the help of Lemma 4, the real part and imaginary part are derived to be independent. Therefore, $F_u(k)$ obeys a noncentral Chi-square distribution with two degrees of freedom. By means of the mean and variance formulas of noncentral Chi-square distribution, the mean and variance of $F_u(k)$ can be achieved as Eqs. (36) and (37).

By virtue of Lemma 5, the power spectrum lines of the same segment are asymptotically uncorrelated. Considering the normality of $X_u(k)$, $X_u(p)$ and $X_u(q)$ are asymptotically independent. Since the continuous function of two independent variables is also independent, $F_u(k)=|X_u(k)|^2$ are independent of different k.

3.3. Probability of false alarm and threshold

In this subsection, using the above conclusions, we construct a novel test statistic $r(l)$. The distribution of test statistic $r(l)$ is derived for calculating the probability of false alarm P_{f} and threshold γ.

From Theorem 1 and Theorem 2, $F_u(k), k=1,2,\ldots,M/2$ of the same segment are independent under both $\mathscr{H}_1$ and $\mathscr{H}_0$. Given $x_u(n)$ are independent at different segment u, the same frequency bins of power spectrum from different segments are also independent. We further derive that $F_{\mathrm{avg}}(k)$,

$k = 1, 2, ..., M/2$ are independent of each other. For a succinct description, we assume that PU transmits the same signal $s(n)$ in different time segments. With the distribution of $F_u(k)$ in the last subsection, the stochastic properties of $F_{\text{avg}}(k)$ are given by

$$E\left[F_{\text{avg}}(k)\,|\mathscr{H}_0\right] = \sigma_\omega^2, \tag{38}$$

$$D\left[F_{\text{avg}}(k)\,|\mathscr{H}_0\right] = \sigma_\omega^4/U, \tag{39}$$

$$E\left[F_{\text{avg}}(k)|\mathscr{H}_1\right] = \frac{\mu_h^2\,|S_u(k)|^2 + G(k)\sigma_h^2}{M} + \sigma_\omega^2, \tag{40}$$

$$D\left[F_{\text{avg}}(k)|\mathscr{H}_1\right] = \frac{\left(G(k)\sigma_h^2 + M\sigma_\omega^2\right)^2}{UM^2} + \frac{2\mu_h^2\,|S_u(k)|^2\left(G(k)\sigma_h^2 + M\sigma_\omega^2\right)}{UM^2}. \tag{41}$$

Since $F_{\text{avg}}(k)$, $k = 1, 2, ..., M/2$ are independent, the distribution of the sum of the power spectrum can be concluded in using the central limit theorem (CLT) when the number of power spectrum bins participating in the operation is sufficiently large (commonly larger than 20).

Thus, F_{full} from Eq. (8) and F_l from Eq. (9) obey a Gaussian distribution

$$F_l \sim \begin{cases} \mathscr{N}\left(E\left[F_l|\mathscr{H}_0\right], D\left[F_l|\mathscr{H}_0\right]\right), & \mathscr{H}_0, \\ \mathscr{N}\left(E\left[F_l|\mathscr{H}_1\right], D\left[F_l|\mathscr{H}_1\right]\right), & \mathscr{H}_1, \end{cases} \tag{42}$$

where

$$E\left[F_l|\mathscr{H}_0\right] = T\sigma_\omega^2/2, \tag{43}$$

$$D\left[F_l|\mathscr{H}_0\right] = T\sigma_\omega^4/2U, \tag{44}$$

$$E\left[F_l|\mathscr{H}_1\right] = \sum_k \left[\frac{\left(\mu_h^2|S_u(k)|^2 + G(k)\sigma_h^2\right)}{M} + \sigma_\omega^2\right], \tag{45}$$

$$D\left[F_l|\mathscr{H}_1\right] = \frac{1}{UM^2}\sum_k\left[\left(G(k)\sigma_h^2 + M\sigma_\omega^2\right)^2 + 2\mu_h^2|S_u(k)|^2\left(G(k)\sigma_h^2 + M\sigma_\omega^2\right)\right], \tag{46}$$

with $k \in [(l-1)T/2+1, lT/2]$ and $l = 1, 2, ..., L$. By the same token, we have

$$F_{\text{full}} \sim \begin{cases} \mathscr{N}\left(E\left[F_{\text{full}}|\mathscr{H}_0\right], D\left[F_{\text{full}}|\mathscr{H}_0\right]\right), & \mathscr{H}_0, \\ \mathscr{N}\left(E\left[F_{\text{full}}|\mathscr{H}_1\right], D\left[F_{\text{full}}|\mathscr{H}_1\right]\right), & \mathscr{H}_1, \end{cases} \tag{47}$$

where

$$E\left[F_{\text{full}}|\mathscr{H}_0\right] = M\sigma_\omega^2/2, \tag{48}$$

$$D\left[F_{\text{full}}|\mathscr{H}_0\right] = M\sigma_\omega^4/2U, \tag{49}$$

$$E\left[F_{\text{full}}|\mathscr{H}_1\right] = \sum_{k=1}^{M/2}\left[\frac{\left(\mu_h^2|S_u(k)|^2 + G(k)\sigma_h^2\right)}{M} + \sigma_\omega^2\right], \tag{50}$$

$$D\left[F_l|\mathscr{H}_1\right] = \frac{1}{UM^2}\sum_{k=1}^{M/2}\left[\left(G(k)\sigma_h^2 + M\sigma_\omega^2\right)^2 + 2\mu_h^2|S_u(k)|^2\left(G(k)\sigma_h^2 + M\sigma_\omega^2\right)\right]. \tag{51}$$

To find the distribution of the test statistic $r(l)$, we give the following theorem.

Theorem 3 If independent random variables A and B obey a Gaussian distribution, the cumulative distribution function (CDF) of $Z = A/B$ is

$$F_Z(z) = \frac{1}{2} + \frac{1}{2}\text{erf}\left(\frac{\mu_B z - \mu_A}{\sqrt{2\left[\sigma_B^2 z^2 + \sigma_A^2\right]}}\right), \tag{52}$$

where μ_A, μ_B, σ_A^2, and σ_B^2 are the mean and variance of A and B, respectively, and $\text{erf}(\cdot)$ is the Gauss error function,

$$\text{erf}(x) = \frac{2}{\sqrt{\pi}}\int_0^x \text{e}^{-\eta^2}\,\text{d}\eta.$$

Proof See Appendix D.

Based on Theorem 3, if $A > 0$, $B > 0$, and $z > 0$, the distribution of $B/(A+B)$ can be further derived as

$$P\left(\frac{B}{A+B} > z\right) = P\left(\frac{A}{B} > \frac{1}{z} - 1\right) = F_Z\left(\frac{1}{z} - 1\right). \tag{53}$$

When we define $B = F_l$ and $A = (F_{\text{full}} - F_l)$, the false alarm probability of the l-th subband can be obtained

$$P_{\text{f},l} = P\left(\frac{F_l}{F_{\text{full}}} > \gamma|\mathscr{H}_0\right) = P\left(\frac{B}{A+B} > \gamma|\mathscr{H}_0\right) = \frac{1}{2} + \frac{1}{2}\text{erf}\left(\frac{E\left[F_l|\mathscr{H}_0\right]/\gamma - E\left[F_{\text{full}}|\mathscr{H}_0\right]}{\sqrt{2D\left[F_l|\mathscr{H}_0\right]\left(\frac{1}{\gamma} - 1\right)^2 + 2\left(\sqrt{D\left[F_{\text{full}}|\mathscr{H}_0\right]} - \sqrt{D\left[F_l|\mathscr{H}_0\right]}\right)^2}}\right). \tag{54}$$

Substituting Eqs. (43), (44), (48), and (49) into Eq. (54), $P_{\text{f},l}$ can be simplified as

$$P_{\text{f},l} = P(r(l) > \gamma|\mathscr{H}_0) = \frac{1}{2} + \frac{1}{2}\text{erf}\left(\frac{T - M\gamma}{2\gamma\sqrt{\frac{T}{U}\left(\frac{1}{\gamma} - 1\right)^2 + \frac{\left(\sqrt{M} - \sqrt{T}\right)^2}{U}}}\right). \tag{55}$$

The false alarm probability of the PSC can be got from L identical to $P_{\mathrm{f},l}$ with the "or" combination rule

$$P_{\mathrm{f}} = 1-(1-P_{\mathrm{f},l})^{L}. \tag{56}$$

Hence, according to the Neyman–Pearson criteria, we can first get $P_{\mathrm{f},l}$ from the preset P_{f}, and then we calculate the decision threshold by substituting $T = M/L$ and $P_{\mathrm{f},l}$ into Eq. (55). The threshold of the PSC can be expressed as follows:

$$\gamma = \frac{1}{L} + \frac{2\sqrt{UM(L-1)\left[\mathrm{erf}^{-1}\left(1-2P_{\mathrm{f},l}\right)\right]^{2} - 4(L-1)\left[\mathrm{erf}^{-1}\left(1-2P_{\mathrm{f},l}\right)\right]^{4}}}{UML - 4L\left[\mathrm{erf}^{-1}\left(1-2P_{\mathrm{f},l}\right)\right]^{2}}, \tag{57}$$

where $\mathrm{erf}^{-1}(x)$ is the inverse function of $\mathrm{erf}(x)$.

4. Performance analysis

In this section, some of the performance including detection probability, suppression of noise uncertainty, computational complexity, and real time analysis will be given. These conclusions will offer a valuable and precise insight into the performance of this algorithm under various channel models and operational scenarios.

4.1. Detection probability

Similar to false alarm probability, equation (58) shows the detection probability of each segment $P_{\mathrm{d},l}$

$$P_{\mathrm{d},l} = \frac{1}{2} + \frac{1}{2}\mathrm{erf}\left(\frac{E\left[F_l|\mathscr{H}_1\right]/\gamma - E\left[F_{\mathrm{full}}|\mathscr{H}_1\right]}{\sqrt{2D\left[F_l|\mathscr{H}_1\right](1/\gamma-1)^{2} + 2\left(\sqrt{D\left[F_{\mathrm{full}}|\mathscr{H}_1\right]} - \sqrt{D\left[F_l|\mathscr{H}_1\right]}\right)^{2}}}\right). \tag{58}$$

From Eq. (11) the final detection probability is

$$P_{\mathrm{d}} = 1 - \prod_{l=1}^{L}(1-P_{\mathrm{d},l}). \tag{59}$$

We can obtain probability in different channels by substituting the corresponding μ_h and σ_h^2 into Eqs. (45), (46), (50), and (51). These theoretical values will be validated in the subsequent section.

4.2. Suppression of noise uncertainty

From the process of the PSC and the threshold expression in Eq. (57), we know that the threshold γ is only related to the segment number U, the segment length M, the subband number L, and the false alarm probability $P_{\mathrm{f},l}$. It is notable that the noise power σ_ω^2 does not exist in Eq. (57). So the PSC threshold γ can be accurately computed from the parameters we previously set. The major advantage of the proposed methods over energy detection is summarized as follows: energy detection needs the noise power for its decision while the proposed method does not. As a blind detection method, the PSC can overcome noise uncertainty perfectly, which is one of the key issues in spectrum sensing.

4.3. Computational complexity

In the following, we will compare the computational complexity of the PSC, energy detection, and eigenvalue-based spectrum sensing. Here we assume N being the sample number for the three methods mentioned above, M is the segment length, and L' is the smoothing factor in eigenvalue-based spectrum sensing.

In energy detection, only N multiplications and $N-1$ additions are needed for one spectrum sensing. In eigenvalue-based spectrum sensing, NL' multiplications and $(N-1)L'$ additions are used for the computation of the covariance matrix. Eigenvalue decomposition need $O(L'^3)$ multiplications and additions. In the PSC, a total of $(N\log_2 M)/2$ multiplications and $N\log_2 M + N$ additions are needed. Where $(N\log_2 M)/2$ multiplications and $(N\log_2 M)$ additions are used for fast Fourier transformation (FFT) in Step 1, N multiplications and $N-M$ additions are used for periodogram spectrum estimation in Step 2, and M additions are used to get the full band power and subband power in Step 3. In sum, energy detection has the lowest computational complexity among the three methods. The PSC and eigenvalue-based spectrum sensing have the same order of computational complexity, both need $O(N)$ multiplications and $O(N)$ additions.

4.4. Real time analysis

From the above text, we know that the computational complexity of the PSC is mainly determined by FFT operations. As the base of digital signal processing, FFT has been implemented in many matured Intellectual Property (IP) cores. By using these IP cores, the real time character of the PSC will be improved remarkably.

The PSC detector is composed of an analog to digital con-

verter (ADC), FFT module, modular square module, split cancellation module, and decision module. Here we take an example of the PSC with $N = 4096$. It delays 1 clk to get one sample from $x(t)$, where clk is the clock cycle. By using the streaming data flow engine architecture IP core of the Altera Company, FFT only needs 4096 clk[26] to output valid transformed data. The modular square module yields one power spectrum lines per clk. The split cancellation module takes 4096 clk in calculating subband power and full band power, and it will take 2 clk for the decision module to compute test statistics and make decisions. If the segment number $U = 1$, the whole process needs almost 8196 clk, such as figure 1 shows.

With 370-MHz clock frequency, it only takes 22.16 μs. If SUs sensing is continuous, by adopting pipeline technology, the PSC needs only 4096 clk, which is 11.068 μs for another 4096 samples sensing.

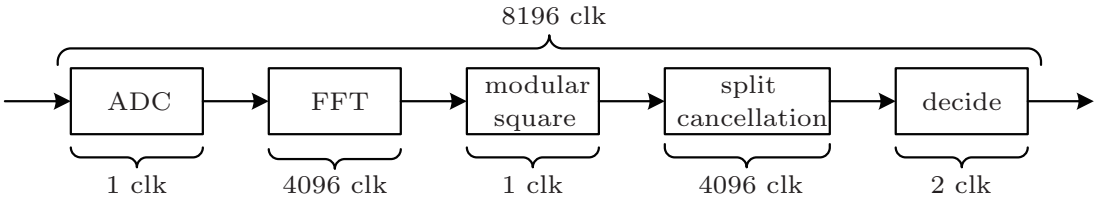


Fig. 1. Real time analysis of PSC method.

5. Simulation results

In this section, we evaluate the performance of the PSC by simulations. Parameters setting will be shown first, and then we provide the simulation results and illustrations.

5.1. Parameters setting

In the following simulations, we choose BPSK signals as the PU transmitting signal. It is necessary to point out that the PSC can be useful for not only BPSK signals but also all the other digital modulation signals. The carrier frequency f_c here is 4.25 MHz, and the symbol rate s_r is 1 MBaud. To avoid aliasing, the sample rate f_s is set as 10 MSPS. The symbol number for sensing is 400, so the number of samples N is 4000. The noise level n_0 is -100 dBm/kHz, and the noise variance (noise power) σ_ω^2 is equal to $n_0 f_s$. If we assume the signal amplitude is A_m, SNR can be defined as $(A_m^2/2n_0 f_s)_{dB}$. When there exists noise uncertainty, noise variance is no longer a constant, but an evenly distributed random variable in interval $[\sigma_\omega^2/\rho, \sigma_\omega^2\rho]$, where ρ is the noise uncertainty factor and $\rho \geq 1$. Without loss of generality, we set the subbands number $L = 4$ and segment number $U = 1$. For credibility of comparison, the smoothing factor of maximum–minimum eigenvalue (MME) detection in Ref. [14] is chosen as 10, which is the optimal one. All the results we provided are averaged over 10^5 Monte Carlo realizations.

5.2. Simulation results

Figure 2 shows the detection probability P_d of the PSC, ED, and MME with different SNRs. The SNR ranges from -12 dB to 0 dB. It was shown that the detection probability P_d of energy detection is the best without noise uncertainty. However, when considering the effect of noise uncertainty, the detection probability P_d of energy detection drops seriously, even the noise uncertainty factor ρ is only 1.05. Much better than energy detection, the PSC still works well with noise uncertainty; the two curves of the PSC with and without noise uncertainty are almost overlapping, which validate Eq. (57) that the PSC is not affected by the noise level. Comparing the PSC and MME detection with the optimal parameters, the curves are very close. MME detection with optimal parameters is only a little better, even less than 0.1 dB under the simulation conditions.

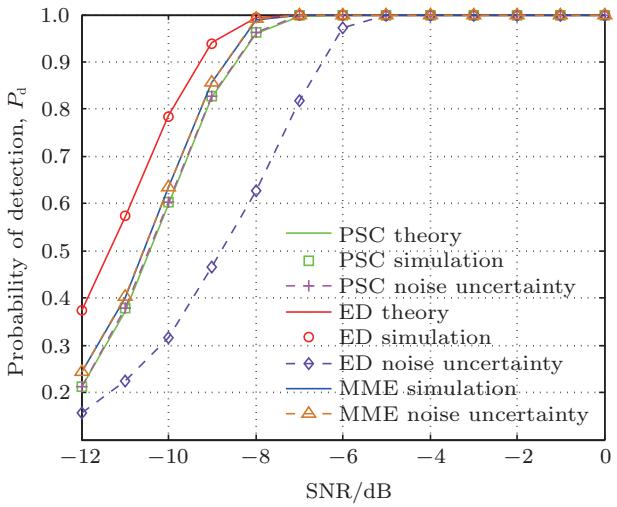


Fig. 2. (color online) Probability of detection of PSC, ED, and MME.

The receiver operating characteristic (ROC) curves are shown in Fig. 3. The probability of false alarm P_f is from 10^{-3} to 10^{-1}, and SNR $= -9$ dB. When there exists noise uncertainty, detection probability P_d of the PSC is the same as that without noise uncertainty, which is much better than energy detection. Besides, at different P_f, the theory results are the same as the simulation results, which validate the threshold γ

we derived in Eq. (57).

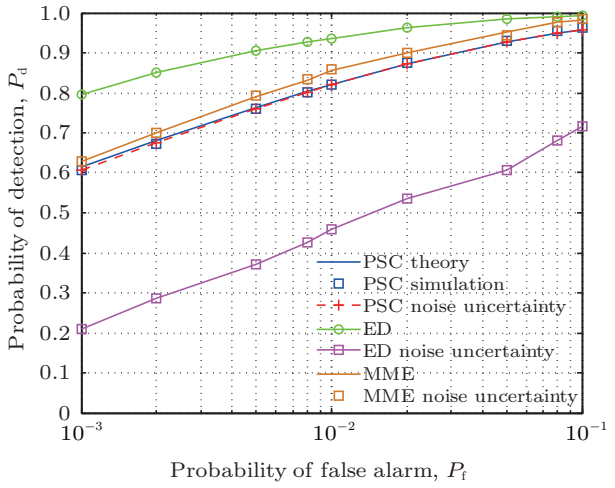


Fig. 3. (color online) ROC curves of PSC, ED, and MME.

Figure 4 provides the ROC curves under fading channels at SNR $= -7$ dB, and the Rician factor is 1. Here we change the samples $N = 2000$ only for distinguishing purposes. It is shown that the curves of the PSC under slow fading channels are a little lower than that under the AWGN channel. The curve of the Rician channel is between the curves of the AWGN channel and the Rayleigh channel. For distinguishing different curves, we only provide the curve with Rician factor 1. It is worth noting that the theoretical detection probability P_d under fading channels is accurate, due to the fact that the simulation results coincide with the theoretical results.

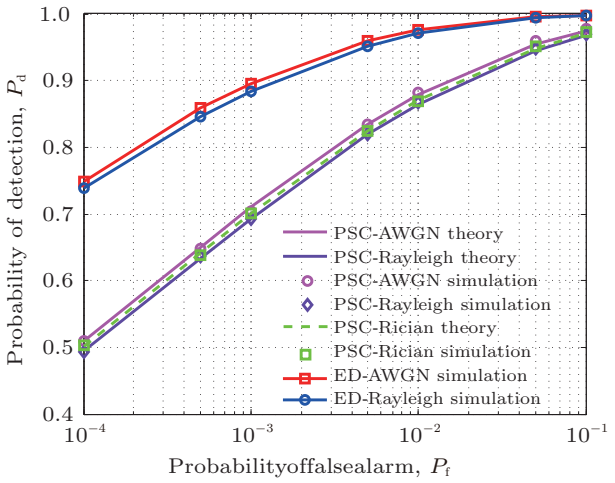


Fig. 4. (color online) ROC curves of the PSC and ED under fading channels.

Figure 5 illustrates the probability of detection under different parameters including segment numbers M, different subband numbers L, and different sample numbers $N = MU$. The plot reveals that the higher number of samples improves the detection performance. Under the simulation condition, when the same samples are divided into more segments, the probability of detection P_d will be improved to some degree. Moreover, more subbands will bring on a little higher performance.

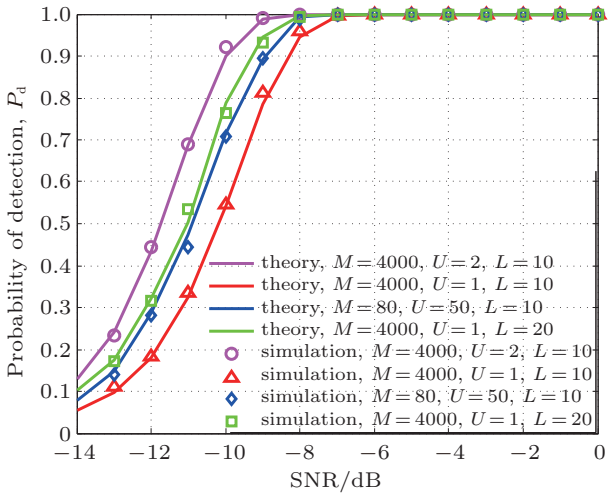


Fig. 5. (color online) Probability of detection of the PSC under different parameters.

6. Conclusions

In this paper, a new spectrum sensing method named PSC is proposed. The ratio of each subband power to the full band power is used as a test statistic inventively, and rigorous closed-form mathematical expressions for the probability of false alarm and detection are calculated by making use of the stochastic properties of discrete samples. Analytical and simulation results show that the PSC has the inherent advantages of invulnerability to noise uncertainty and the PSC could offer a high probability of detection at a low probability of false alarm for a wide range of SNR in different channels without prior knowledge. Meanwhile, the proposed method has a low computational complexity, which can be completed in microseconds. For these reasons, the PSC, a robust spectrum sensing method, has potential applicability in piratical CR systems. Moreover, as a bonus, we can apply the PSC to distinguish multiple signals, which are not aliasing in an ultra-wideband.

Appendix A: Proof of Lemma 3

Under $\mathscr{H}_1$, the mean of $X_u^{\mathrm{r}}(k)$ is

$$\begin{aligned} & E\left[X_u^{\mathrm{r}}(k)\right] \\ &= E\left[\frac{1}{\sqrt{M}}\sum_{n=0}^{M-1}\cos\left(\frac{2\pi}{M}kn\right)\left(\omega_u^{\mathrm{r}}(n)+h_u^{\mathrm{r}}(n)s_u(n)\right)\right. \\ &\quad \left.+\frac{1}{\sqrt{M}}\sum_{n=0}^{M-1}\sin\left(\frac{2\pi}{M}kn\right)\left(\omega_u^{\mathrm{i}}(n)+h_u^{\mathrm{i}}(n)s_u(n)\right)\right]. \end{aligned} \tag{A1}$$

Substituting Eq. (15) into Eq. (A1) results in

$$E\left[X_u^{\mathrm{r}}(k)\right] = \frac{1}{\sqrt{M}}\sum_{n=0}^{M-1}\cos\left(\frac{2\pi}{M}kn\right)s_u(n)E\left[h_u^{\mathrm{r}}(n)\right]$$

$$+\frac{1}{\sqrt{M}}\sum_{n=0}^{M-1}\sin\left(\frac{2\pi}{M}kn\right)s_u(n)E\left[h_u^{\mathrm{i}}(n)\right]$$
$$=\frac{1}{\sqrt{M}}\mu_h^{\mathrm{r}}S_u^{\mathrm{r}}(k)+\frac{1}{\sqrt{M}}\mu_h^{\mathrm{i}}S_u^{\mathrm{i}}(k). \quad (A2)$$

The variance of $X_u^{\mathrm{r}}(k)$ under $\mathscr{H}_1$ can be expressed as

$$D\left[X_u^{\mathrm{r}}(k)\right]$$
$$=D\left[\frac{1}{\sqrt{M}}\sum_{n=0}^{M-1}\cos\left(\frac{2\pi}{M}kn\right)\left(\omega_u^{\mathrm{r}}(n)+h_u^{\mathrm{r}}(n)s(n)\right)\right.$$
$$\left.+\frac{1}{\sqrt{M}}\sum_{n=0}^{M-1}\sin\left(\frac{2\pi}{M}kn\right)\left(\omega_u^{\mathrm{i}}(n)+h_u^{\mathrm{i}}(n)s(n)\right)\right]. \quad (A3)$$

Considering the independence between $h(n)$ and $\omega(n)$, the variance of $X_u^{\mathrm{r}}(k)$ can be simplified when replacing Eq. (16) into Eq. (A3)

$$D\left[X_u^{\mathrm{r}}(k)\right]=\frac{\sigma_\omega^2}{2}+\frac{1}{M}D\left[\sum_{n=0}^{M-1}\cos\left(\frac{2\pi}{M}kn\right)s(n)h_u^{\mathrm{r}}(n)\right.$$
$$\left.+\sum_{n=0}^{M-1}\sin\left(\frac{2\pi}{M}kn\right)s(n)h_u^{\mathrm{i}}(n)\right]. \quad (A4)$$

As independent variables $h_u^{\mathrm{r}}(n)$ and $h_u^{\mathrm{i}}(n)$ have the same variance, we can obtain

$$D\left[X_u^{\mathrm{r}}(k)\right]$$
$$=\frac{\sigma_h^2}{2M}\left[\sum_{n'=0}^{M/R-1}\left|\sum_{n=0}^{R-1}s\left(Rn'+n\right)\exp\left(\frac{-2\pi\mathrm{j}k(Rn'+n)}{M}\right)\right|^2\right]$$
$$+\frac{\sigma_\omega^2}{2}$$
$$=\frac{\sigma_\omega^2}{2}+\frac{\sigma_h^2G(k)}{2M}, \quad (A5)$$

where $G(k)$ is given by Eq. (33). In the same way, the mean and variance of $X_u^{\mathrm{i}}(k)$ can be obtained.

Appendix B: Proof of Lemma 4

By making use of similar replacements, the covariance between $X_u^{\mathrm{r}}(k)$ and $X_u^{\mathrm{i}}(k)$ under $\mathscr{H}_1$ can be calculated as

$$\mathrm{Cov}\left[X_u^{\mathrm{r}}(k),X_u^{\mathrm{i}}(k)\right]$$
$$=E\left[X_u^{\mathrm{r}}(k)X_u^{\mathrm{i}}(k)\right]-E\left[X_u^{\mathrm{r}}(k)\right]E\left[X_u^{\mathrm{i}}(k)\right]$$
$$=E\left[\frac{1}{\sqrt{M}}\left\{\sum_{n=0}^{M-1}s(n)\left[\cos\left(\frac{2\pi kn}{M}\right)h_u^{\mathrm{r}}(n)\right.\right.\right.$$
$$\left.\left.+\sin\left(\frac{2\pi kn}{M}\right)h_u^{\mathrm{i}}(n)\right]\right\}$$
$$\times\frac{1}{\sqrt{M}}\left\{\sum_{n=0}^{M-1}s(n)\left[\cos\left(\frac{2\pi kn}{M}\right)h_u^{\mathrm{i}}(n)\right.\right.$$
$$\left.\left.\left.-\sin\left(\frac{2\pi kn}{M}\right)h_u^{\mathrm{r}}(n)\right]\right\}\right]$$
$$-\left[\mu_h^{\mathrm{i}}S^{\mathrm{r}}(k)-\mu_h^{\mathrm{r}}S^{\mathrm{i}}(k)\right]\left[\mu_h^{\mathrm{r}}S^{\mathrm{r}}(k)+\mu_h^{\mathrm{i}}S^{\mathrm{i}}(k)\right]$$
$$=\left[\mu_h^{\mathrm{i}}S^{\mathrm{r}}(k)-\mu_h^{\mathrm{r}}S^{\mathrm{i}}(k)\right]\left[\mu_h^{\mathrm{r}}S^{\mathrm{r}}(k)+\mu_h^{\mathrm{i}}S^{\mathrm{i}}(k)\right]$$
$$+S^{\mathrm{r}}(k)S^{\mathrm{i}}(k)\left(\sigma_h^2/2-\sigma_h^2/2\right)$$
$$-\left[\mu_h^{\mathrm{i}}S^{\mathrm{r}}(k)-\mu_h^{\mathrm{r}}S^{\mathrm{i}}(k)\right]\left[\mu_h^{\mathrm{r}}S^{\mathrm{r}}(k)+\mu_h^{\mathrm{i}}S^{\mathrm{i}}(k)\right]$$
$$=0. \quad (B1)$$

Appendix C: Proof of Lemma 5

The covariance between $X_u(p)$ and $X_u(q)$ is given below

$$\mathrm{Cov}[X_u(p),X_u(q)]$$
$$=E\left[\overline{\langle X_u(p)-E\left(X_u(p)\right)\rangle}\left\langle X_u(q)-E\left(X_u(q)\right)\right\rangle\right]$$
$$=E\left[\overline{\left(\frac{1}{\sqrt{M}}\sum_{n=0}^{M-1}\exp\left(\frac{-2\pi\mathrm{j}pn}{M}\right)\left(h_u(n)s(n)+\omega_u(n)\right)\right)}\right.$$
$$\left.\times\left(\frac{1}{\sqrt{M}}\sum_{v=0}^{M-1}\exp\left(\frac{-2\pi\mathrm{j}qv}{M}\right)\left(h_u(v)s(v)+\omega_u(v)\right)\right)\right]$$
$$-E\left[\overline{X_u(p)}\right]E\left[X_u(q)\right]$$
$$=\frac{1}{M}E\left[\left(\sum_{n'=0}^{M/R-1}\left\{\exp\left(\frac{-2\pi\mathrm{j}pn'}{M}\right)T\left(-p\right)T\left(q\right)\right\}\right)\right]\sigma_h^2, \quad (C1)$$

where

$$T\left(p\right)=\sum_{n=0}^{R-1}s(Rn'+n)\exp\left(\frac{-2\pi\mathrm{j}pn}{M}\right),$$
$$T\left(q\right)=\sum_{v=0}^{R-1}s(Rv'+v)\exp\left(\frac{-2\pi\mathrm{j}qv}{M}\right).$$

The correlation coefficient can be further derived

$$|\rho|=\left|\frac{\mathrm{Cov}[X_u(p),X_u(q)]}{\sqrt{D[X_u(p)]}\sqrt{D[X_u(q)]}}\right|$$
$$=\frac{\frac{1}{M}\left|\sum_{n'=0}^{M/R-1}\exp\left(\frac{-2\pi\mathrm{j}pn'}{M}\right)T\left(-p\right)T\left(q\right)\right|\sigma_h^2}{\sqrt{\frac{1}{M}G\left(p\right)\sigma_h^2+\sigma_\omega^2}\sqrt{\frac{1}{M}G\left(q\right)\sigma_h^2+\sigma_\omega^2}}$$
$$\le\frac{\sigma_h^2\sum_{n'=0}^{M/R-1}\left[\left|\exp\left(\frac{-2\pi\mathrm{j}pn'}{M}\right)\right||T\left(-p\right)||T\left(q\right)|\right]}{\sqrt{G\left(p\right)\sigma_h^2+M\sigma_\omega^2}\sqrt{G\left(q\right)\sigma_h^2+M\sigma_\omega^2}}$$
$$=\frac{\sigma_h^2\sum_{n'=0}^{M/R-1}\left[|T\left(-p\right)||T\left(q\right)|\right]}{\sqrt{G\left(p\right)\sigma_h^2+M\sigma_\omega^2}\sqrt{G\left(q\right)\sigma_h^2+M\sigma_\omega^2}}$$

$$\leq \frac{\sigma_h^2 \sum_{n'=0}^{M/R-1} [|T(-p)||T(q)|]}{\left(\sigma_h^2 + \frac{1}{\mathrm{SNR}}\right)\sqrt{G(P)G(q)}}$$
$$\leq \frac{\sigma_h^2}{\sigma_h^2 + \frac{1}{\mathrm{SNR}}} \to 0\,(\mathrm{SNR} \to 0)\,, \tag{C2}$$

where $G(p)$ and $G(q)$ were given in Eq. (33).

Appendix D: Proof of Theorem 3

If independent random variables A and B obey a Gaussian distribution, the distribution of $Z = A/B$ is

$$\begin{aligned} F_Z(z) &= \mathrm{Prob}\left(\frac{A}{B} < z\right) \\ &= 1 - \mathrm{Prob}\left(\frac{A}{B} > z\right) \\ &= 1 - \int_{-\infty}^{\infty}\int_{bz}^{\infty} f_A(a)\,\mathrm{d}a f_B(b)\,\mathrm{d}b \\ &= 1 - \int_{-\infty}^{\infty}\int_{bz}^{\infty} \frac{\exp\left(-\frac{(a-\mu_A)^2}{2\sigma_A^2}\right)}{\sqrt{2\pi}\sigma_A}\,\mathrm{d}a \\ &\quad \times \frac{\exp\left(-\frac{(b-\mu_B)^2}{2\sigma_B^2}\right)}{\sqrt{2\pi}\sigma_B}\,\mathrm{d}b. \end{aligned} \tag{D1}$$

By setting $t = (a-\mu_A)/\sqrt{2}\sigma_A$, we have

$$\begin{aligned} F_Z(z) &= 1 - \frac{\sqrt{2\pi}}{4\pi\sigma_B}\int_{-\infty}^{\infty}\left[1 - \mathrm{erf}\left(\frac{bz-\mu_A}{\sqrt{2}\sigma_A}\right)\right] \\ &\quad \times \exp\left(-\frac{(b-\mu_B)^2}{2\sigma_B^2}\right)\mathrm{d}b. \end{aligned} \tag{D2}$$

Setting $c = (b-\mu_B)/\sqrt{2}\sigma_B$,

$$\begin{aligned} F_Z(z) &= 1 - \frac{1}{2\sqrt{\pi}}\int_{-\infty}^{\infty}\exp\left(-c^2\right)\mathrm{d}c \\ &\quad + \frac{1}{2\sqrt{\pi}}\int_{-\infty}^{\infty}\left\{\mathrm{erf}\left(\frac{\sigma_B z c}{\sigma_A} + \frac{\mu_B z - \mu_A}{\sqrt{2}\sigma_A}\right)\right\} \\ &\quad \times \exp\left(-c^2\right)\mathrm{d}c. \end{aligned} \tag{D3}$$

From Eqs. (3.321) and (8.259) in Ref. [27], we obtain

$$F_Z(z) = \frac{1}{2} + \frac{1}{2}\mathrm{erf}\left(\frac{\mu_B z - \mu_A}{\sqrt{2\left[\sigma_B^2 z^2 + \sigma_A^2\right]}}\right). \tag{D4}$$

References

[1] Akyildiz I F, Lee W Y, Vuran M C and Mohanty S 2006 *Comput. Networks* **50** 2127

[2] Zheng S, Kam P, Liang Y and Zeng Y 2013 *IEEE Trans. Wireless Commun.* **12** 1774

[3] Haykin S 2005 *IEEE Select. Areas Commun.* **23** 201

[4] Zu Y X, Zhou J and Zeng C C 2010 *Chin. Phys. B* **19** 119501

[5] Zu Y X and Zhou J 2012 *Chin. Phys. B* **21** 019501

[6] De P and Liang Y C 2008 *IEEE Trans. Veh. Technol.* **57** 2834

[7] Axell E, Leus G, Larsson E G and Poor H V 2012 *IEEE Signal Process. Mag.* **29** 101

[8] Liu Y, Peng Q C, Shao H Z, Peng Q H and Wang L 2013 *Acta Phys. Sin.* **62** 078406 (in Chinese)

[9] Zheng S L, Lou C Y and Yang X N 2010 *Acta Phys. Sin.* **59** 3611 (in Chinese)

[10] Cordeiro C, Challapali K, Birru D and Sai S N 2005 *First IEEE International Symposium on New Frontiers in Dynamic Spectrum Access Networks*, Baltimore, November 8-11, 2005, p. 328

[11] Shen L, Wang H, Zhang W and Zhao Z 2011 *IEEE Trans. Wireless Commun.* **10** 1721

[12] Sahai A, Hoven N and Tandra R 2004 *Proc. Allerton Conf. Commun., Control, Comput.*, Monticello, October 3–7, 2004, p. 11

[13] Lundén J, Koivunen V, Huttunen A and Poor H V 2009 *IEEE Trans. Signal Process.* **57** 4182

[14] Zeng Y H and Liang Y C 2009 *IEEE Trans. Commun.* **57** 1784

[15] Zeng Y H and Liang Y C 2009 *IEEE Trans. Veh. Technol.* **58** 1804

[16] Bianchi P, Debbah M, Maida M and Najim J 2011 *IEEE Trans. Inf. Theory* **57** 2400

[17] Kortun A, Ratnarajah T, Sellathurai M, Zhong C J and Papadias C B 2011 *IEEE J. Select. Topics Signal Process.* **5** 49

[18] Penna F, Garello R, Figliloli D and Spirito M A 2009 *Proc. 4th Int. Conf. Cognitive Radio Oriented Wireless Netw. Commun.*, June 16–18, 2009, Hannover, Germany, p. 1

[19] Urkowitz H 1967 *Proc. IEEE* **55** 523

[20] Axell E and Larsson G E 2011 *IEEE J. Select. Areas Commun.* **29** 290

[21] Gismalla E H 2011 *IEEE Trans. Signal Process.* **59** 3712

[22] Friman O, Volosyak I and Graser A 2007 *IEEE Trans. Biomed. Eng.* **54** 742

[23] Quan Z, Cui S, Sayed A H and Poor H V 2009 *IEEE Trans. Signal Process.* **57** 1128

[24] Qi P H, Li Z, Si J B and Gao R 2013 *Journal of Xidian University* **40** 19 (in Chinese)

[25] Tandra R and Sahai A 2008 *IEEE J. Select. Topics Signal Process.* **2** 4

[26] Altera http://www.altera.com 2012-11

[27] Gradshteyn I and Ryzhik I 2007 *Table of Integrals, Series, and Products*, 7th edn. (New York: Academic Press) pp. 276–278